Hindawi
Journal of Nanomaterials
Volume 2023, Article ID 1312288, 8 pages
https://doi.org/10.1155/2023/1312288

Research Article

Synthesis and Characterization of Zinc, Iron, Copper, and Manganese Oxides Nanoparticles for Possible Application as Plant Fertilizers

Michel E. Neto,[1] **David W. Britt**,[2] **Kyle A. Jackson**,[2] **João H. V. Almeida Junior**,[1] **Rodrigo S. Lima**,[1] **Dimas A. M. Zaia**,[3] **Tadeu T. Inoue**,[1] **and Marcelo A. Batista**[1]

[1]*Agronomy Department, Maringá State University, Maringá 87020-900, Paraná, Brazil*
[2]*Biological Engineering Department, Utah State University, Logan, UT 84322, USA*
[3]*Chemistry Department, Londrina State University, Londrina 86057-970, Paraná, Brazil*

Correspondence should be addressed to Michel E. Neto; michelesper14@gmail.com

Received 26 September 2022; Revised 1 February 2023; Accepted 9 February 2023; Published 23 February 2023

Academic Editor: Osman Ahmed Zelekew

This research evaluates the synthesis and characterization of nanometric-sized metallic particles with potential application as support materials for supplying nutrients to plants. Nanoscale Zn, Mn, Fe, and Cu oxides particles were synthesized using microwave-assisted synthesis. Nanoparticles (NPs) were characterized with Fourier transform infrared (FTIR) spectroscopy, X-ray diffraction (XRD), transmission electron microscopy (TEM), thermogravimetric analysis (TGA), specific surface area (SSA), and total chemical analysis. Synthesized NPs were all in oxide forms and characterized for confirmation of size, shape, surface structure, crystalline nature, and study of elemental proportion. The results indicate that synthesized NPs size was ranged between 20 and 50 nm and was all in their respective oxide forms as ZnO, Mn_3O_4, Fe_3O_4, and CuO.

1. Introduction

Nanoparticles (NPs) are all those particles which present at least one dimension <100 nm, and normally show properties not found in bulk particles with the same molecular composition [1]. Industries of NPs are developing metal and metal oxides for the improvement of their services and products. The reported applications of these kind of particles have grown in all science areas like food technology, pharmacy, medicine, engineering, and even though agriculture, mainly, due its advances in chemical synthesis methodologies [2], in which, with other synthesis techniques may become easier and faster to produce nanoparticle.

Because of their high energy content on surface, NPs are very reactive and thermodynamic unstable [3]. Therefore, there are several interests to synthesize, develop, and commercialize NP [4, 5]. Despite the positive benefits caused by NP, there is also a concern related to their toxicological effects to human [6, 7] and plants [8].

Nanoparticles usually differ from their bulk particles exhibiting different physiochemical properties like optical, thermal, and/or electrical [9]. Normally, NPs are built by addition of reducing or precipitating agents during their synthesis [10]. Several factors are responsible for NP reactivity, including size, core composition, shape, surface properties, purity, stability, and method of manufacturing [9]. NPs can be synthesized through physical, chemical, and biological reactions. In the physical reaction, the reduction of a bulk material into smaller particles (nanometer size) occurs through milling, vaporization, and laser ablation. In the chemical reaction, molecules, atoms, or small particles join, becoming larger particles [11, 12]. In biological synthesis, different microorganisms are used to form NPs through enzymatic reactions [13]. Among manufacturing methods, microwave-assisted synthesis has been used to produce oxide NP [14, 15]. This simple method shows some advantages when compared to conventional heating. The advantages of

using microwaves are due to homogeneous heating throughout the synthesis process, allowing rapid formation of NP [15]. Furthermore, it is an effective technique for the preparation of nanoparticles. And as a disadvantage, the technique has a shorter crystallization time and homogeneous nucleation due to the uniform heat of the microwave oven [16].

In agriculture, NP may be used as nanofertilizer (NF). NF is proposed to enhance nutrient efficiency used by plants, delivering in an "on-demand manner" [17]. This practice promotes efficient way to avoid repeated and exceeding applications of conventional fertilizers, which may cause environmental problems due to their high solubility of conventional fertilizers [18, 19]. In addition, these losses also generate financial expenses and, consequently, negative impacts to any society inserted around these activities.

The elements usually studied as NF are zinc (Zn), iron (Fe), copper (Cu), and manganese (Mn) because these elements are essential micronutrient to plants, and are often applied as soluble salts. Nevertheless, micronutrient availability to the plants applied may become low and deficiency occurs in some soils with alkaline pH, sandy texture, or those with low organic matter content [20].

Presumably, NF can improve the solubility and dispersion of insoluble nutrients in the soil, reduce fixation, and increase nutrient availability [19]. In order to increase the productive capacity of agricultural areas for the coming years, one of the trends has been the development and use of new fertilizer technologies. Therefore, NF has been shown to improve the efficiency of fertilizer use by several researchers. Thus, this work aimed to quickly and cheaply synthesize and characterize Fe, Zn, Mn, and Cu NPs so that they can be later used as a source of micronutrients for cultivated plants.

2. Materials and Methods

2.1. Chemicals. The chemicals used in the experiment, iron sulfate heptahydrate ($FeSO_4{\cdot}7H_2O$), zinc sulfate ($ZnSO_4{\cdot}7H_2O$), manganese sulfate ($MnSO_4{\cdot}H_2O$), copper sulfate ($CuSO_4{\cdot}5H_2O$), and sodium hydroxide (NaOH), were purchased from Merck Chemicals Ltd. (Merck KGaA, Darmstadt, Germany) and were stored according to the supplier's instructions and used as received.

2.2. Synthesis of Nanoparticles. All oxides in this research were synthesized from the coprecipitation with the 0.4 mol L^{-1} alkaline NaOH solution. The $FeSO_4{\cdot}7H_2O$, $ZnSO_4{\cdot}7H_2O$, $MnSO_4{\cdot}H_2O$, and $CuSO_4{\cdot}5H_2O$ reagents, all in the concentration of 0.1 mol L^{-1}, were used as precursors for the formation of Fe, Zn, Cu, and Mn nanoparticles, respectively.

NaOH 0.4 mol L^{-1} solution of 100 mL and saline solution 0.1 mol L^{-1} ($FeSO_4{\cdot}7H_2O$, $ZnSO_4{\cdot}7H_2O$, $MnSO_4{\cdot}H_2O$, $CuSO_4{\cdot}5H_2O$) of 100 mL were prepared and subsequently mixed slowly dropwise (saline solutions) in 500 mL Erlenmeyer flask. Thereafter, the solution was stirred vigorously on a magnetic stirrer at 1,500 rpm in a temperature-controlled environment at 20°C for 15 uninterrupted minutes. The reaction flask was put to the microwave oven *Brastemp 38* L (model BMJ38ARANA) for 2.5 min at a power of 300 W. Subsequently, the reaction flask was cooled in a temperature-controlled environment at 20°C.

After these procedures, the precipitate was formed in each reaction flask. The flasks were then washed several times with ultrapure water (*Milli-Q*) to remove excess SO_4^{2-} and Na^+ remaining in solution. The washed precipitate was frozen instantaneously at −70°C in liquid nitrogen, dried by sublimation in *Terroni* LS 3000 lyophilizer, packed under a vacuum glass desiccator, and protected from light.

2.3. Characterization Techniques. The synthesized NPs were measured by X-ray diffraction (XRD), *Shimadzu* diffractometer using CoKα radiation where $\lambda = 0.179$ nm with a nickel filter (35 kV, 20 mA) between 20° and 75° 2θ in the transmission mode for step of 0.01° 2θ/0.6 s. The mean crystallite dimension (D) was broken through the most intense peak using the *Debye–Scherrer* presentation. The size and shape of the NPs were obtained through transmission electron microscopy (TEM) using a *Philips EM300* transmission electron microscope operated at 80 kV with a tungsten filament. Samples were prepared by dispersing 0.05 g in 30 mL of ultrapure water and dispersing by ultrasonic vibration (Bandelin Sonoplus D-12207). The dispersions were placed in a 200 mesh polyvinyl *formvar*-coated grade and allowed to dry in a temperature-controlled environment.

The total contents of Cu, Fe, Mn, and Zn observed in the NPs were acquired through total chemical analysis, where 100 mg of each NP sample was dissolved by adding 3 mL of concentrated H_2SO_4. Grades were determined using the *Agilent*® microwave plasma-atomic emission spectrometer (*MP-AES*). Expected and observed Fe, Zn, Mn, and Cu contents were calculated based on the amounts of Fe, Zn, Mn, and Cu used in the synthesis and the values obtained in the total chemical analysis, respectively, according to the synthesized mineral identified by XRD. Thermogravimetric analysis (TGA) studies were carried out using the *Shimadzu DT-60H* equipment, where samples were obtained from a temperature of 25–1,000°C with a heating rate of 10° min^{-1} under an air atmosphere. Specific surface area (SSA) was measured by *Brunauer–Emmett–Teller* (BET) particle absorption isotherms on *Micromeritics FlowSorb II 2300* [21]. Fourier transform infrared (FTIR) spectroscopy was recorded on a 200 mg KBr disk in a *Shimadzu* FTIR model 8300 spectrophotometer with a spectral resolution of 4 cm^{-1}. FTIR spectra were recorded in the range of 400–4,000 cm^{-1}.

3. Results and Discussion

The XRD pattern of the ZnO NP powder is shown in Figure 1(a). From this analysis of XRD patterns, peak intensity, position, and width were determined. The XRD peaks were found at positions at 36.98°, 40.14°, 42.27°, 55.75°, 66.73°, and 74.43° 2θ; these peaks are characteristic and indexed as hexagonal zincite (ZnO), ICDD 050664, with lattice constants of $a = b = 0.3254$ and $c = 0.5213$ nm. The average diameter of the crystallite formed in the process was estimated from the *Debye–Scherrer* equation ($d = K\,(\lambda/\beta \cos\theta)$) using the diffraction peak corresponding to the (101) plane located at 42.27° 2θ, resulting in an average value of 26.6 nm.

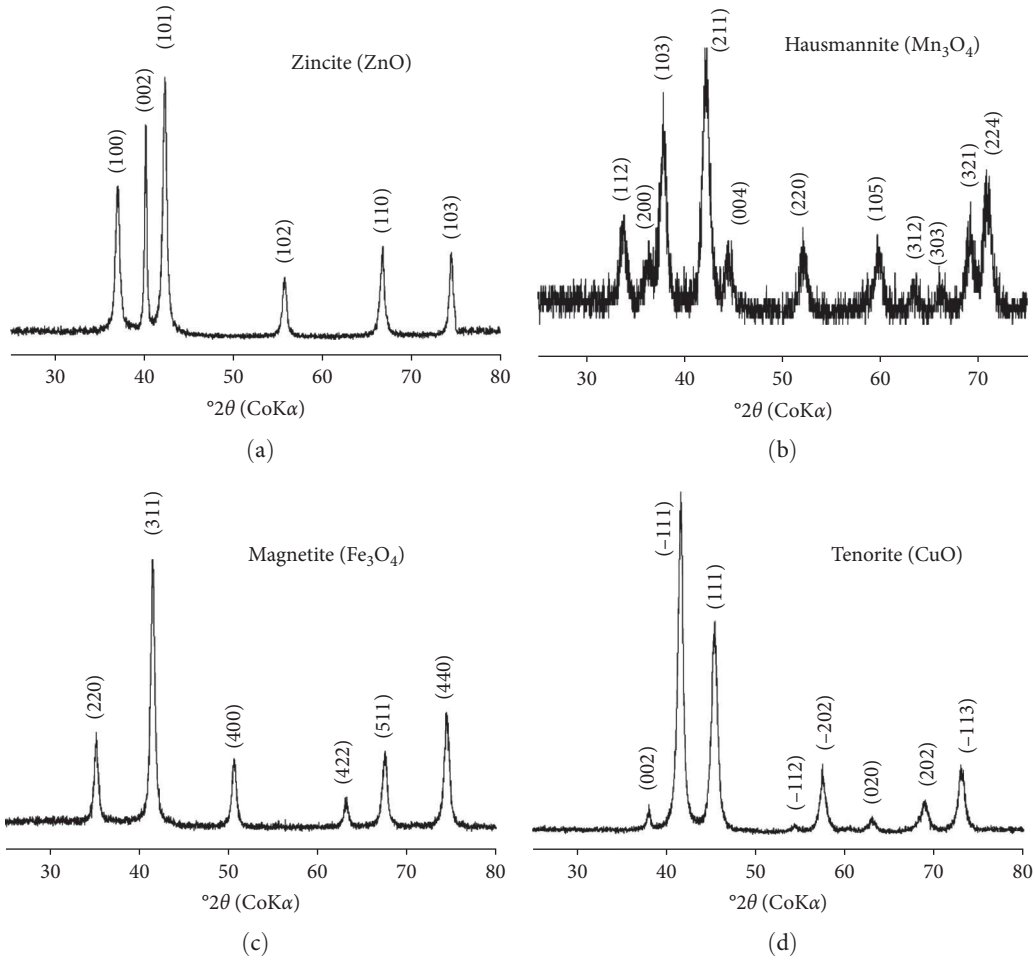

Figure 1: Nanoparticle (NP) X-ray diffraction: (a) Zn NP (zincite-ZnO); (b) Mn NP (hausmannite-Mn_3O_4); (c) Fe NP (magnetite-Fe_3O_4); (d) Cu NP (tenorite-CuO).

Figure 1(b) shows the XRD pattern obtained from the powdered samples of Mn_3O_4 NP. The XRD peaks were found at positions at 33.66°, 37.76°, 42.14°, 44.61°, 51.99°, 59.82°, 69.09°, and 70° 2θ; these peaks are characteristic and indexed as hausmannite (Mn_3O_4), ICDD 240734, of tetragonal phase, with lattice constants of $a = b = 0.5762$ and $c = 0.9423$ nm. *Debye–Scherrer* emission showed that the mean crystallite size was 32.8 nm.

Figure 1(c) shows the XRD pattern of the powdered samples of the Fe NP. Analyzing the diffractogram, the peak intensity, position, and width were determined, total width at half maximum. The XRD peaks were found at positions at 35.26°, 41.55°, 50.69°, 63.23°, 67.60°, and 74.73° 2θ. The relative position and intensity of the peaks correspond to the characteristic peaks and indexed as cubic phase of magnetite (Fe_3O_4), ICDD 890691, with lattice constants of $a = b = c =$ 0.8375 nm. The particle size according to the *Scherrer* equation was 14.1 nm.

The diffractogram of the CuO powder material NP is shown in Figure 1(d). Peak intensity, position, and width were determined. The XRD peaks were found at positions at 41.33°, 41.53°, 57.21°, 68.89°, and 72.91° 2θ. The relative position and intensity of the peaks correspond to the characteristic peaks and indexed as tenorite (CuO), ICDD 050661, of monoclinic crystals, with lattice constants of $a = 0.4522$, $b = 0.3302$, and $c = 0.5157$ nm. The particle size according to *Scherrer's* equation was 35.27 nm.

Table 1: Total chemical analysis of synthetic nanofertilizers of Cu, Fe, Mn, and Zn.

MO	Expected (mol %)	Observed (mol %)	SD (mol %)	Observed/expected (%)
CuO	79.9	78.7	0.3	99.8
Fe_3O_4	72.4	66.0	1.5	91.2
Mn_3O_4	72.0	70.3	1.2	97.6
ZnO	80.4	74.2	0.2	92.3

MO, metal oxide; SD, standard deviation.

Cu, Fe, Mn, and Zn contents observed in the synthesized NP were 0.2%, 8.8%, 2.4%, and 7.7% lower than expected (Table 1). The expected contents for CuO, Fe_3O_4, Mn_3O_4, and ZnO were 79.9%, 72.4%, 72.0%, and 80.4%, and the observed values were 78.7%, 66.0%, 70.3%, and 74.3%, respectively. The SSA, measured by the BET method, of the synthetic NP was 43.74, 54.62, 106.45, and 38.68 $m^2\ g^{-1}$ for CuO, Fe_3O_4,

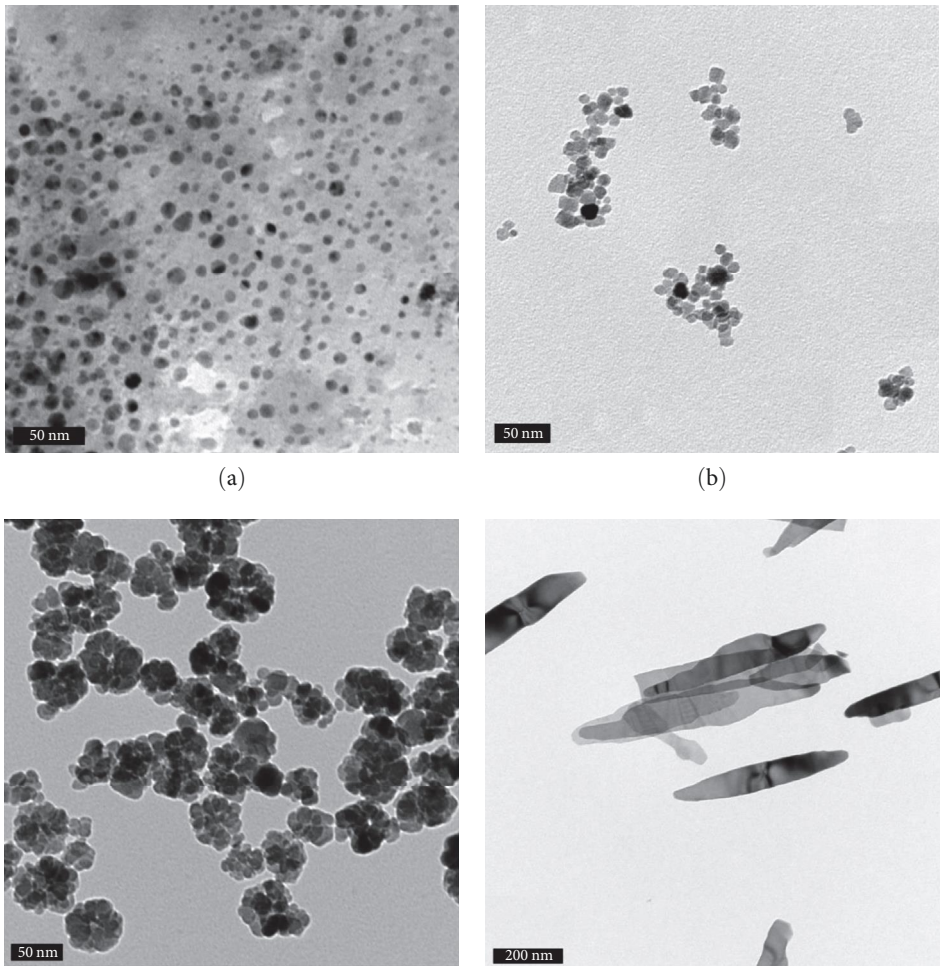

Figure 2: Transmission electron microscopy (TEM) of the synthesized particles: (a) ZnO < 20 nm; (b) Mn_3O_4 < 20 nm; (c) Fe_3O_4 < 20 nm; (d) CuO with length >100 nm and width <50 nm.

Mn_3O_4, and ZnO, respectively. Figure 2 shows TEM images of all nanoparticles synthesized.

Regarding FTIR results, the ZnO band at 3,163 cm^{-1} is due to OH stretching of hydroxyl group, probably due to adsorbed water. It should be noted that this band vanished when the samples were heated at temperatures higher than 600°C (Figure 3(a)) [22, 23]. The bands in the region from 600 to 1,700 cm^{-1} are due to CO_2 (g) from the air. The bands at region from 629 to 745 cm^{-1}, 845 cm^{-1} (sharp), and 1,187/1,303 cm^{-1} are attributed to in-plane deformation of CO_3^{2-}, out-of-plane deformation of CO_3^{2-}, and symmetric/asymmetric stretch of CO_3^{2-} [24]. The absorption peak associated with Zn–O stretching band clearly appears at 503 cm^{-1} confirming the formation of ZnO NP [25].

For Mn_3O_4, the bands at 3,400 (broad) and 1,640 cm^{-1} could be attributed to OH stretching and OH bending, respectively (Figure 3) [26, 27]. The band at 656 cm^{-1} could be attributed to Mn–O stretching or SO_4^{2-} bending [24, 27]. These bands are attributed to interaction of SO_4^{2-} forming a bidentate binuclear (bridging) surface complex with Mn_3O_4 [28].

For Fe_3O_4, the bands at 3,397 (broad) and 1,644 cm^{-1} could be attributed to OH stretching and OH bending, respectively [29]. The bands at 898, 796, and 629 cm^{-1} could be attributed to OH in-plane bending, OH out-of-plane bending, and Fe–O symmetric stretching, respectively [30]. The bands at 898 and 796 cm^{-1} are characteristic of goethite. However, X-ray diffractogram (Figure 3(c)) did not show any characteristic peak of goethite, probably because FTIR spectroscopy is a much more sensitive technique than X-ray diffractometry.

For CuO, the bands at 3,402 (wide) and 1,643 cm^{-1} reveal the presence of OH elongation and OH bending for the alkyl group. The bands at 1,370 and 1,096 cm^{-1} are characteristic bands of Cu NPs due to Cu^{2+}, $-O^{2-}$, and SO_4^{2-} stretching [28, 31]. The band attributed to SO elongation of SO_4^{2-} is very weak, meaning that very low concentration of SO_4^{2-} adsorbed onto CuO. Furthermore, single band means that SO_4^{2-} is interacting with CuO as a sphere complex [28].

Figure 4(a) shows TGA of ZnO NP. A high rate of mass loss was observed between 30 and 100°C. A high rate of ZnO mass loss was observed in the initial stages when the water adsorbed on the surface of the NP evaporates [32]. The second phase of water loss around 350°C occurs due to decomposition and is associated with the rupture of weak

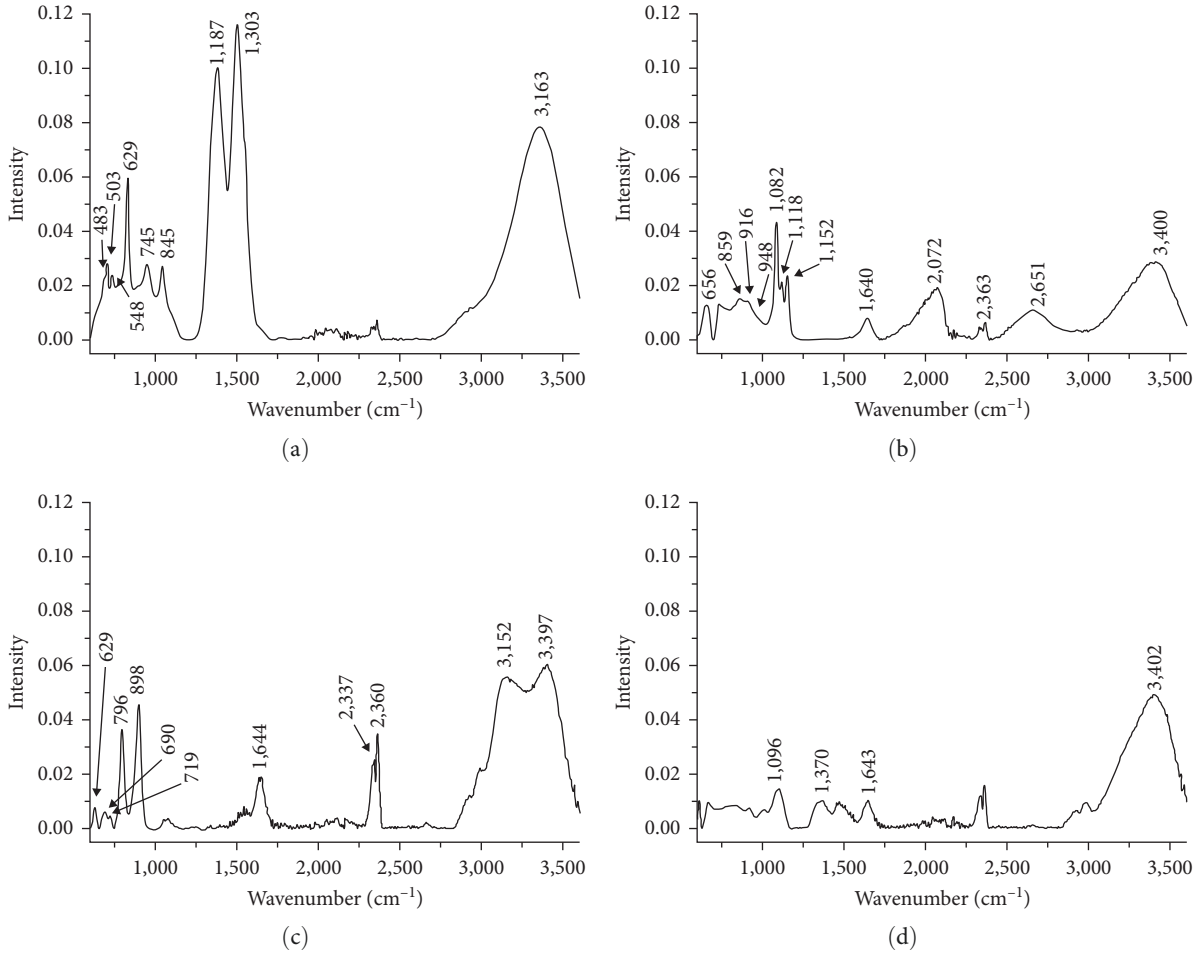

Figure 3: FTIR spectrum of (a) ZnO NP, (b) Mn_3O_4 NP, (c) Fe_3O_4 NP, and (d) CuO NP.

bonds and unpacking of highly strained crosslinks, resulting in the formation of straight $Zn(OH)_2$ chains [33]. After 470°C, the aggregation of ZnO NP is expected because the exposed irradiated microwaves increase the surface energy of ZnO NP [34].

The thermal behavior of Mn NP through the TGA technique is shown in Figure 4(b). There are two mass losses: the first up to 100°C and the other above 500°C. The mass loss at 100°C is due to the evaporation of water absorbed on the surface of Mn_3O_4. Furthermore, above 500°C, Mn_3O_4 will be converted into Mn_2O_3 [35]. The gradual weight loss above 100°C can be attributed to the superficial sintering of Mn_3O_4 NP, although the reason for this phenomenon is still unclear [36].

The mass loss for Fe_3O_4 was 5.7% for the entire temperature range due to physical and chemical water removal from adsorbed water (100–130°C) (Figure 4(c)). When Fe_3O_4 is brought to high temperatures, products containing O_2 may occur by oxidation reactions of magnetite into hematite ($4Fe_3O_4 + O_2 \longrightarrow 6Fe_2O_3$) [37]. The mass loss of CuO suggests, first, up to 150°C, losses caused by evaporation of free and coordinated water in CuO NP. The second mass loss between 250 and 400°C is due to the removal of counter anions in gases [38] through dehydration and pyrolysis. Above 400°C, weight loss may be due to loss of oxygen (Figure 4(d)).

The NPs synthesis process through the microwave use was efficient. The method was quick and simple. Several authors for the synthesis of oxides, hydroxides, and oxyhydroxides nanoparticles [39] have already demonstrated the efficiency of the microwave-assisted method. The benefits of this method in relation to the hydrothermal method are: (1) rapid reaction, (2) simple method, (3) short time to reach the appropriate temperature for the reaction, and (4) the morphology of the particles is in control [15]. In addition, XRD diffractogram (Figure 1) shows that the powdered particles have low impurity contents, since they did not present with any other peak that is not present in the zincite, hausmannite, tenorite, and magnetite diffractograms.

The presence of other elements composing the minerals or the incomplete formation of the minerals may explain this subtle difference between the observed and expected contents of the elements (Table 1). The SSA values found for ZnO in this work are larger than other ZnO synthetic nanoparticles [40, 41] and slightly lower [42]. Regarding Mn_3O_4, which was the highest BET value found in this work, but despite that, BET values were lower ($177.6\,m^2\ g^{-1}$) [43].

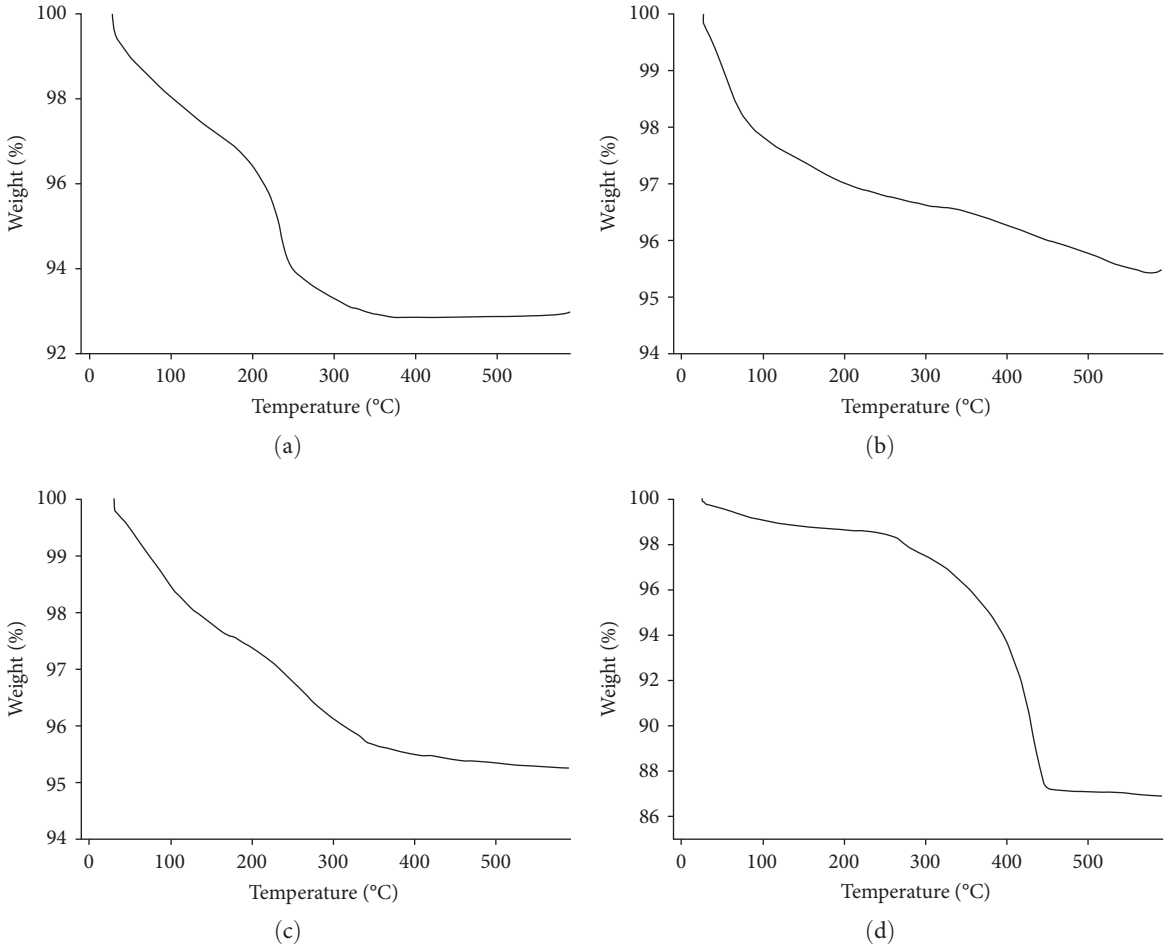

Figure 4: Thermal analysis spectrum of (a) ZnO NP, (b) Mn_3O_4 NP, (c) Fe_3O_4 NP, and (d) CuO NP.

It was found that SSA varies between 7.3 and 104 $m^2\ g^{-1}$ for Fe_3O_4 [44]; therefore, the results obtained by authors mention that the synthesis by different routes of precipitation and degree of oxidation alter the particle size. The values of SSA found in this work for CuO were higher [19, 45], even though within an acceptable size range.

ZnO particles are well separated from each other, and it is also evident in the dark field that each particle is a single crystal of rounded shape [46]. The particle size shown by TEM was lower than 20 nm, showing a very narrow size distribution, which is characteristic of mechanically synthesized particles [47]. The estimated XRD size using the Scherrer equation was 21.3 nm and is well in agreement with the TEM images, since the sizes obtained were similar.

The morphology, structure, and distribution of Mn_3O_4 were described by Chang et al. [48], and some synthesized particles have cubic forms. The particle size shown by TEM was around 20 nm when viewed on a single particle, having a diameter close to that estimated by the Scherrer equation in XRD (26 mm). In general, the size of the Mn_3O_4 particles depends on temperature during the synthesis, which means, the lower the growth temperature, the smaller the particle size [48].

Regarding Fe_3O_4, most of the particles appear to be uniform and spherical in shape. Allied to this, the particles show high aggregation capacity. The preparation of the sample to be analyzed in the MET may be one of the reasons that induce colloid aggregation [49]. The size of the individual particles is shown to have a diameter of about 20 nm, like the diameter estimated by XRD using the Scherrer equation.

CuO morphology is thin and pointed like needle or wires [50]. The aggregation is lower than the Cu particle when compared to the Fe and Mn particles, even though the Cu particles are larger when compared to the others. According to the Scherrer equation, the particle has an average size of 31.5 nm, although the TEM image showed that the particles can be up to 100 nm in length.

4. Conclusion

It was possible to synthesize nanoparticles of Cu, Fe, Zn, and Mn at the nanoscale. The synthesis methodology provided an increasing scale of Zn, Mn, Fe, and Cu sizes, although all particles presented at nanoscale. The characterization methods were efficient to measure the size and quality of synthesized NF.

Data Availability

The data used to support the findings of this study are available from the corresponding author upon request.

Conflicts of Interest

The authors declare that they have no conflicts of interest.

References

[1] M. Auffan, J. Rose, J.-Y. Bottero, G. V. Lowry, J.-P. Jolivet, and M. R. Wiesner, "Towards a definition of inorganic nanoparticles from an environmental, health and safety perspective," *Nature Nanotechnology*, vol. 4, pp. 634–641, 2009.

[2] J. A. Gerbec, D. Magana, A. Washington, and G. F. Strouse, "Microwave-enhanced reaction rates for nanoparticle synthesis," *Journal of the American Chemical Society*, vol. 127, no. 45, pp. 15791–15800, 2005.

[3] J.-P. Jolivet, C. Froidefond, A. Pottier et al., "Size tailoring of oxide nanoparticles by precipitation in aqueous medium. A semi-quantitative modelling," *Journal of Materials Chemistry*, vol. 14, no. 21, pp. 3281–3288, 2004.

[4] A. K. Gupta and M. Gupta, "Synthesis and surface engineering of iron oxide nanoparticles for biomedical applications," *Biomaterials*, vol. 26, no. 18, pp. 3995–4021, 2005.

[5] J.-Y. Bottero, J. Rose, and M. R. Wiesner, "Nanotechnologies: tools for sustainability in a new wave of water treatment processes," *Integrated Environmental Assessment and Management*, vol. 2, no. 4, pp. 391–395, 2006.

[6] G. Oberdörster, E. Oberdörster, and J. Oberdörster, "Nanotoxicology: an emerging discipline evolving from studies of ultrafine particles," *Environmental Health Perspectives*, vol. 113, no. 7, pp. 823–839, 2005.

[7] A. Nel, T. Xia, L. Mädler, and N. Li, "Toxic potential of materials at the nanolevel," *Science*, vol. 311, no. 5761, pp. 622–627, 2006.

[8] D. Lin and B. Xing, "Root uptake and phytotoxicity of ZnO nanoparticles," *Environmental Science & Technology*, vol. 42, no. 15, pp. 5580–5585, 2008.

[9] A. Rastogi, M. Zivcak, O. Sytar et al., "Impact of metal and metal oxide nanoparticles on plant: a critical review," *Frontiers in Chemistry*, vol. 5, Article ID 78, 2017.

[10] M. Sanchez-Dominguez, M. Boutonnet, and C. Solans, "A novel approach to metal and metal oxide nanoparticle synthesis: the oil-in-water microemulsion reaction method," *Journal of Nanoparticle Research*, vol. 11, pp. 1823–1829, 2009.

[11] P. G. Jamkhande, N. W. Ghule, A. H. Bamer, and M. G. Kalaskar, "Metal nanoparticles synthesis: an overview on methods of preparation, advantages and disadvantages, and applications," *Journal of Drug Delivery Science and Technology*, vol. 53, Article ID 101174, 2019.

[12] N. Rajput, "Methods of preparation of nanoparticles—a review," *International Journal of Advances in Engineering & Technology*, vol. 7, no. 4, pp. 1806–1811, 2015.

[13] R. L. Karnani and A. Chowdhary, "Biosynthesis of silver nanoparticle by eco-friendly method," *Indian Journal of Nanoscience*, vol. 1, pp. 25–31, 2013.

[14] D. Sharma, S. Sharma, B. S. Kaith, J. Rajput, and M. Kaur, "Synthesis of ZnO nanoparticles using surfactant free in-air and microwave method," *Applied Surface Science*, vol. 257, no. 22, pp. 9661–9672, 2011.

[15] M. Hasanpoor, M. Aliofkhazraei, and H. Delavari, "Microwave-assisted synthesis of zinc oxide nanoparticles," *Procedia Materials Science*, vol. 11, pp. 320–325, 2015.

[16] A. Ali, H. Zafar, M. Zia et al., "Synthesis, characterization, applications, and challenges of iron oxide nanoparticles," *Nanotechnology, Science and Applications*, vol. 9, pp. 49–67, 2016.

[17] P. Wang, E. Lombi, F.-J. Zhao, and P. M. Kopittke, "Nanotechnology: a new opportunity in plant sciences," *Trends in Plant Science*, vol. 21, no. 8, pp. 699–712, 2016.

[18] M. E. Trenkel, *Slow- and Controlled-Release and Stabilized Fertilizers: An Option for Enhancing Nutrient Use Efficiency in Agriculture*, International Fertilizer Industry Association, Paris, France, 2010.

[19] R. Liu and R. Lal, "Potentials of engineered nanoparticles as fertilizers for increasing agronomic productions," *Science of The Total Environment*, vol. 514, pp. 131–139, 2015.

[20] N. K. Fageria, *The Use of Nutrients in Crop Plants*, CRC Press, Boca Raton, 2009.

[21] S. Brunauer, P. H. Emmett, and E. Teller, "Adsorption of gases in multimolecular layers," *Journal of The American Chemical Society*, vol. 60, no. 2, pp. 309–319, 1938.

[22] A. K. Zak, W. H. A. Majid, M. Darroudi, and R. Yousefi, "Synthesis and characterization of ZnO nanoparticles prepared in gelatin media," *Materials Letters*, vol. 65, no. 1, pp. 70–73, 2011.

[23] K. Sowri Babu, A. Ramachandra Reddy, C. Sujatha, K. Venugopal Reddy, and A. N. Mallika, "Synthesis and optical characterization of porous ZnO," *Journal of Advanced Ceramics*, vol. 2, pp. 260–265, 2013.

[24] N. B. Colthup, L. H. Daly, and S. E. Wiberley, *Introduction to Infrared and Raman Spectroscopy*, Academic Press Inc., 1990.

[25] T. Khalafi, F. Buazar, and K. Ghanemi, "Phycosynthesis and enhanced photocatalytic activity of zinc oxide nanoparticles toward organosulfur pollutants," *Scientific Reports*, vol. 9, Article ID 6866, 2019.

[26] A. Vázquez-Olmos, R. Redón, G. Rodríguez-Gattorno et al., "One-step synthesis of Mn_3O_4 nanoparticles: structural and magnetic study," *Journal of Colloid and Interface Science*, vol. 291, no. 1, pp. 175–180, 2005.

[27] A. K. M. Atique Ullah, A. K. M. Fazle Kibria, M. Akter et al., "Synthesis of Mn_3O_4 nanoparticles via a facile gel formation route and study of their phase and structural transformation with distinct surface morphology upon heat treatment," *Journal of Saudi Chemical Society*, vol. 21, no. 7, pp. 830–836, 2017.

[28] D. Peak, R. G. Ford, and D. L. Sparks, "An *in situ* ATR-FTIR investigation of sulfate bonding mechanisms on goethite," *Journal of Colloid and Interface Science*, vol. 218, no. 1, pp. 289–299, 1999.

[29] K. Raees, M. S. Ansari, and M. Z. A. Rafiquee, "Inhibitive effect of super paramagnetic iron oxide nanoparticles on the alkaline hydrolysis of procaine," *Journal of Nanostructure in Chemistry*, vol. 9, pp. 175–187, 2019.

[30] R. M. Cornell and U. Schwertmann, *The Iron Oxides: Structure, Properties, Reactions, Occurences and Uses, Second Edition*, Wiley-VCH, Weinheim, 2003.

[31] V. Prakash, R. K. Diwan, and U. K. Niyogi, "Characterization of synthesized copper oxide nanopowders and their use in nanofluids for enhancement of thermal conductivity," *Indian Journal of Pure & Applied Physics*, vol. 53, no. 11, pp. 753–758, 2015.

[32] A. H. Moharram, S. A. Mansour, M. A. Hussein, and M. Rashad, "Direct precipitation and characterization of ZnO nanoparticles," *Journal of Nanomaterials*, vol. 2014, Article ID 716210, 5 pages, 2014.

[33] F. A. López, M. I. Martín, F. J. Alguacil, J. M. Rincón, T. A. Centeno, and M. Romero, "Thermolysis of fibreglass

polyester composite and reutilisation of the glass fibre residue to obtain a glass–ceramic material," *Journal of Analytical and Applied Pyrolysis*, vol. 93, pp. 104–112, 2012.

[34] A. Pimentel, D. Nunes, P. Duarte et al., "Synthesis of long ZnO nanorods under microwave irradiation or conventional heating," *The Journal of Physical Chemistry C*, vol. 118, no. 26, pp. 14629–14639, 2014.

[35] M. Ocaña, "Uniform particles of manganese compounds obtained by forced hydrolysis of manganese(II) acetate," *Colloid and Polymer Science*, vol. 278, pp. 443–449, 2000.

[36] C.-L. Liu, K.-H. Chang, C.-C. Hu, and W.-C. Wen, "Microwave-assisted hydrothermal synthesis of Mn_3O_4/reduced graphene oxide composites for high power supercapacitors," *Journal of Power Sources*, vol. 217, pp. 184–192, 2012.

[37] N. Arsalani, H. Fattahi, and M. Nazarpoor, "Synthesis and characterization of PVP-functionalized superparamagnetic Fe_3O_4 nanoparticles as an MRI contrast agent," *eXPRESS Polymer Letters*, vol. 4, no. 6, pp. 329–338, 2010.

[38] P. Deka, R. C. Deka, and P. Bharali, "*In situ* generated copper nanoparticle catalyzed reduction of 4-nitrophenol," *New Journal of Chemistry*, vol. 38, no. 4, pp. 1789–1793, 2014.

[39] J. Zhao, W. Yan, R. Xu, W. Pang, and Q. Huo, "Microwave-assisted inorganic syntheses," in *Modern Inorganic Synthetic Chemistry*, R. Xu, W. Pang, and Q. Huo, Eds., pp. 173–195, Elsevier, Amsterdam, 2011.

[40] J. H. Zeng, B. B. Jin, and Y. F. Wang, "Facet enhanced photocatalytic effect with uniform single-crystalline zinc oxide nanodisks," *Chemical Physics Letters*, vol. 472, no. 1–3, pp. 90–95, 2009.

[41] H. Lu, S. Wang, L. Zhao, J. Li, B. Dong, and Z. Xu, "Hierarchical ZnO microarchitectures assembled by ultrathin nanosheets: hydrothermal synthesis and enhanced photocatalytic activity," *Journal of Materials Chemistry*, vol. 21, no. 12, pp. 4228–4234, 2011.

[42] A. Lei, B. Qu, W. Zhou, Y. Wang, Q. Zhang, and B. Zou, "Facile synthesis and enhanced photocatalytic activity of hierarchical porous ZnO microspheres," *Materials Letters*, vol. 66, no. 1, pp. 72–75, 2012.

[43] T. Yousefi, A. N. Golikand, M. H. Mashhadizadeh, and M. Aghazadeh, "High temperature and low current density synthesis of Mn_3O_4 porous nano spheres: characterization and electrochemical properties," *Current Applied Physics*, vol. 12, no. 2, pp. 544–549, 2012.

[44] J. Mürbe, A. Rechtenbach, and J. Töpfer, "Synthesis and physical characterization of magnetite nanoparticles for biomedical applications," *Materials Chemistry and Physics*, vol. 110, no. 2-3, pp. 426–433, 2008.

[45] K. Zhou, R. Wang, B. Xu, and Y. Li, "Synthesis, characterization and catalytic properties of CuO nanocrystals with various shapes," *Nanotechnology*, vol. 17, no. 15, Article ID 3939, 2006.

[46] T. Tsuzuki and P. G. McCormick, "ZnO nanoparticles synthesised by mechanochemical processing," *Scripta Materialia*, vol. 44, no. 8-9, pp. 1731–1734, 2001.

[47] T. Tsuzuki and P. G. McCormick, "Synthesis of CdS quantum dots by mechanochemical reaction," *Applied Physics A*, vol. 65, pp. 607–609, 1997.

[48] Y. Q. Chang, X. Y. Xu, X. H. Luo, C. P. Chen, and D. P. Yu, "Synthesis and characterization of Mn_3O_4 nanoparticles," *Journal of Crystal Growth*, vol. 264, no. 1–3, pp. 232–236, 2004.

[49] S. Laurent, D. Forge, M. Port et al., "Magnetic iron oxide nanoparticles: synthesis, stabilization, vectorization, physicochemical characterizations, and biological applications," *Chemical Reviews*, vol. 108, no. 6, pp. 2064–2110, 2008.

[50] M. Sahooli, S. Sabbaghi, and R. Saboori, "Synthesis and characterization of mono sized CuO nanoparticles," *Materials Letters*, vol. 81, pp. 169–172, 2012.